HHS Public Access

Author manuscript

Environ Pollut. Author manuscript; available in PMC 2021 April 01.

Published in final edited form as:

Environ Pollut. 2020 April ; 259: 113908. doi:10.1016/j.envpol.2019.113908.

N^6-methyladenosine mediates arsenite-induced human keratinocyte transformation by suppressing p53 activation

Tianhe Zhao[1], **Donglei Sun**[1], **Manyu Zhao**[1], **Yanhao Lai**[2], **Yuan Liu**[2], **Zunzhen Zhang**[1,*]

[1]Department of Environmental and Occupational Health, West China School of Public Health and West China Fourth Hospital, Sichuan University, Chengdu, Sichuan, China, 610041

[2]Department of Chemistry and Biochemistry, Florida International University, Miami, FL, USA, 33199

Abstract

N^6-methyladenosine (m^6A), the most abundant and reversible RNA modification, plays critical a role in tumorigenesis. However, whether m^6A can regulate p53, a leading antitumor protein remains poorly understood. In this study, we explored the regulatory role of m^6A on p53 activation using an arsenite-transformed keratinocyte model, the HaCaT-T cell line. We created the cell line by exposing human keratinocyte HaCaT cells to 1 μM arsenite for 5 months. We found that the cells exhibited an increased m^6A level along with an aberrant expression of the methyltransferases, demethylase, and readers of m^6A. Moreover, the cells exhibited decreased p53 activity and reduced p53 phosphorylation, acetylation, and transactivation with a high nucleus export rate of p53. Knockdown of the m^6A methyltransferase, METTL3 significantly decreased m^6A level, restoring p53 activation and inhibiting cellular transformation phenotypes in the arsenite-transformed cells. Further, using both a bioinformatics analysis and experimental approaches, we demonstrated that m^6A downregulated the expression of the positive p53 regulator, PRDM2, through the YTHDF2-promoted decay of PRDM2 mRNAs. We showed that m^6A upregulated the expression of the negative p53 regulator, YY1 and MDM2 through YTHDF1-stimulated translation of YY1 and MDM2 mRNA. Taken together, our study revealed the novel role of m^6A in mediating arsenite-induced human keratinocyte transformation by suppressing p53 activation. This study further sheds light on the mechanisms of arsenic carcinogenesis via RNA epigenetics.

[*]**Corresponding author:** Zunzhen Zhang, Ph.D., Sichuan University West China School of Public Health and West China Fourth Hospital, Chengdu, Sichuan, China, zhangzunzhen@163.com; zhangzz@scu.edu.cn, Tel: +86-028-85501298, Fax: +86-028-85501295.

Author contributions

Tianhe Zhao designed and performed the experiments and conducted data analysis. Donglei Sun prepared the draft figures and conducted the data analyses. Tianhe Zhao and Manyu Zhao drafted the manuscript. Yanhao Lai revised manuscript. Yuan Liu provided suggestions for the study design and reconstructed and revised the manuscript. Zunzhen Zhang participated in the study design, reconstructed, and revised the manuscript.

Competing interests

The authors have declared that no competing interests exist.

Declaration of interests

The authors declare that they have no known competing financial interests or personal relationships that could have appeared to influence the work reported in this paper.

Summarizes

Increased m^{6}A attenuates p53 activation in arsenite-transformed human keratinocytes.

Keywords

N^6-methyladenosine; arsenite; p53 activation; cell transformation

Introduction

Arsenite is a widespread environmental pollutant that poses a severe health threat to more than 100 million people worldwide [1,2]. It belongs to one of the Class 1 carcinogens designated by the International Agency for Research on Cancer (IARC) [3]. However, the carcinogenic mechanisms of arsenite remain to be elucidated. A recent study from our group has demonstrated that N^6-methyladenosine (m^{6}A), one of the most abundant and reversible post-transcriptional modifications in eukaryotic RNA, mediates the proliferation and apoptosis of arsenite-transformed human bronchial epithelial cells [4]. This suggests a new mechanistic pathway that leads to arsenite carcinogenesis through m^{6}A. This is further supported by the results from the studies showing that m^{6}A is associated with arsenite-induced oxidative stress [5–7], which is the major cause of its carcinogenicity. Increased m^{6}A promoted the proliferation of human keratinocytes that are exposed to low levels of arsenite, possibly through the inhibition of oxidative stress [5]. Also, it has been found that arsenite-induced oxidative stress can elevate the level of m^{6}A in keratinocytes [6]. All these suggest a new role of m^{6}A in arsenite carcinogenesis. Thus, it is critically important to elucidate the mechanisms by which m^{6}A mediates arsenite-induced carcinogenesis as this can significantly advance our understanding of arsenite carcinogenicity and open a new avenue for prevention of arsenite carcinogenesis.

It has been shown that m^{6}A is also involved in the mutations of the tumor suppressor p53 and regulation of the expression of the genes in the p53 pathway in human cells [8]. In myeloid leukemia patients, the genetic alterations of m^{6}A regulatory genes are associated with p53 gene mutation [9]. In mice, elevated m^{6}A level alters the expressions of 127 genes, among which 78 genes are in the p53 functional interaction network [10]. These suggest a strong association between m^{6}A and activation of the p53 pathway in mammals. Since downregulation of the expression of p53 and its inactivation can mediate arsenite toxicity [11–13], we further hypothesize that m^{6}A mediates arsenite-induced transformation by regulating the expression of p53 and altering its functional activation. To test this hypothesis, in this study, we explored how arsenite can induce cell transformation through the effects of m^{6}A on the p53 expression, activity, and function in human cells using both experimental approaches and bioinformatics analysis of the datasets from several publications.

Given that skin cancer caused by hyperkeratosis is the most common form of cancers induced by arsenite, and cell transformation is a commonly used approach for studying the carcinogenicity of arsenite, we used human keratinocytes that were transformed by chronic arsenite exposure as the model system for this study. We found that m^{6}A mediated arsenite-induced cell transformation by suppressing p53 activation rather than regulating p53 gene

expression. In a combination of the results from both the experiments and bioinformatics analysis, we demonstrated that a high m^6A level inactivated p53 by modulating the expressions of p53 regulators. Our study provides the first evidence that m^6A modification plays a pivotal role in arsenite-induced inactivation of p53, shedding light on a new mechanism by which RNA epigenetics mediates arsenite carcinogenicity.

Materials and Methods

Human keratinocyte culture

The human keratinocyte line (HaCaT) was purchased from KeyGen (Nanjing, China) and cultured by High-glucose Dulbecco's Modified Eagle's Medium (DMEM; Life Technologies, USA) with serum in 37 °C humidified incubator containing 5% CO_2.

Arsenite treatment and short interfering RNA (siRNAs) transfection

HaCaT cells were continuously maintained in the medium containing 0 or 1 μM sodium arsenite ($NaAsO_2$, Sigma, St. Louis, MO, purity: 99.0%) for 50 passages (about 5 months) with 72 h per passage. HaCaT cells treated by 1 μM arsenite for 50 passages were named as HaCaT-T cells. The transformation phenotypes of HaCaT-T cells were characterized by cell proliferation and clone assays. All short siRNAs were synthesized by RIBOBIO (Guangzhou, China). siR-Ribo™ Negative Control (RIBOBIO, Guangzhou, China) was used as siRNA control (siControl). HaCaT cells and HaCaT-T cells were seeded in 6-well plates with antibiotic-free medium at 2×10^5 cells/well. Adherent cells were then transfected with METTL3 siRNAs (siMETTL3–1 and siMETTL3–2), YTHDF1 siRNAs (siYTHDF1–1 and siYTHDF1–2), YTHDF2 siRNAs (siYTHDF2–1 and siYTHDF2–2), and negative control (siControl), respectively using riboFECT™ CP (RIBOBIO, Guangzhou, China). The transfected cells were cultured for 72 h and harvested for experiments.

Cell proliferation and viability assay

Cell proliferation and viability were tested by MTT assay. For the determination of cell proliferation rate, HaCaT cells and HaCaT-T cells were cultured in 96-well plates at a density of 2×10^3 cells/well for 0 h, 24 h, 48 h, 72 h, and 96 h. For the assay on cell viability, 1×10^4 cells were seeded per well in 96-well plates. Adherent cells were exposed to different concentrations of arsenite (0 μM, 5 μM, 10 μM, 15 μM, 20 μM, 40 μM, 60 μM) for 24 h. Cells were then incubated with MTT (0.5 mg/mL) at 37 °C for 4 h in the dark, and formazan crystals were dissolved by dimethylsulfoxide. Absorbance at 570 nm was measured by Multiskan™GO (Thermo Fisher Scientific, Inc., USA). The cell proliferation rate and viability of each group were normalized to the control, respectively.

Cell anchorage-independent growth measured by soft agar clone formation assay

DMEM with 0.6% agar was used as under-layer soft agar in 96-well plate, 1000 cells in DMEM with 0.35% agar were seeded per well in this plate. After incubated at 37 °C for 2 weeks, cell clones (> 75 μm in diameter) were photographed and counted in a microscope (OLYMPUS, Japan). The clone formation percentage was calculated as follows:

$$\text{Clone formation (\%)} = \text{the number of clone}/1000 \times 100\%.$$

Formation of cell clones detected by plate colony formation assay

One thousand cells were seeded per well in 12-well plates and cultured for 10 days. Cells were then washed twice with phosphate-buffered saline (PBS), fixed in methanol for 20 min, and stained with 10% (w/v) Giemsa for 15 min. Colonies that contain 50 or more cells were counted under a microscope (OLYMPUS, Japan). The colony formation percentage was calculated as follows:

$$\text{Colony formation (\%)} = \text{the number of colony}/1000 \times 100\%.$$

Cell migration determined by wound-healing assay

Cells (1×10^6) were seeded per well into 6-well plates to form a confluent monolayer. A wound made by a 200 μL pipet tip, and cells were imaged with microscopy after the wound was made 48 h later. The cell migration areas were analyzed by the ImageJ software (National Institutes of Health, USA). The migration area was calculated as follows:

$$\text{Migration area} = (A_0 - A_{48})/A_0$$

"A_0" is the area of the wound at the beginning. "A_{48}" is the area of the wound after 48 h.

Measurement of cell apoptosis by flow cytometry

Apoptosis was detected by Annexin V- fluorescein isothiocyanate (FITC) Apoptosis Detection Kit (Vazyme Biotech Co. Nanjing, China). Floating and attached cells were resuspended in 500 μL of binding buffer, stained with 5 μL propidium iodide (PI) and 5 μL Annexin V-FITC. Cells were protected from light and incubated at room temperature for 30 min. Apoptotic cells (10,000 cells per sample) were immediately analyzed using flow cytometry (BD FACSVerse, US).

Measurement of mRNA levels by quantitative reverse transcription-PCR (RT-qPCR)

Isolation of total RNA, measurement of the amount of RNA, synthesis of cDNA, and detection of RNA levels were performed as described previously [6]. The sequences of the PCR primers are listed in Supplementary Table 1. RT-qPCR was performed according to the method described previously [6].

Measurement of protein levels in cells by Western blot

Cells were lysed by lysis buffer (Beyotime, China) containing a phosphatase inhibitor (Servicebio, China) and protease inhibitor, PMSF (Roche, China). Proteins were detected and analyzed according to the method described previously [6]. Antibodies against METTL3, METTL14, WTAP, KIAA1429, FTO, YTDHF1, p53 acetyl-lys382, and PRDM2 were from Abcam (Cambridge, UK). Antibodies against p53 and GAPDH were from Proteintech

Group (Wuhan, China). Antibodies against p53 phospho-ser15, phospho-ser46, phospho-ser392, MDM2, and YY1 were from Absin Bioscience Inc. (Shanghai, China).

Measurement of total m^{6}A level

The m^{6}A level in total RNA was detected by EpiQuik m^{6}A RNA Methylation Quantification Kit (Epigentek, Farmingdale, USA) as described previously [6]. Briefly, RNA samples were incubated with an m^{6}A capture antibody with 1:1000 dilution at room temperature for 1 h, and detection antibody with 1:2000 dilution at room temperature for 30 min. Subsequently, the samples were incubated with the enhancer solution and detection solution at room temperature and subject to the measurement of the absorbance at 450 nm using the Multiskan™ GO plate reader. The amount of m^{6}A was calculated according to the equation described previously [6].

Measurement of p53 activity

The p53 activity in the nuclear extract was detected by the Human p53 Activity Assay Kit (GeneCopoeia, Inc, USA). Nuclear proteins of cells were extracted using Nuclear and Cytoplasmic Protein Extraction Kit (MeiLunbio, China). The concentrations of nuclear proteins were measured by BCA Protein Assay Kit (MeiLunbio, China). Subsequently, p53 activity in nuclear extract was detected by Human p53 Activity Assay Kit (GeneCopoeia, Inc, USA). Briefly, 10 μL sample (50 μg of nuclear proteins) was added into each well of a 96-well plate with 50 μL of Binding Buffer A at room temperature for 1 h with gentle rocking. 100 μL diluted p53 primary antibody was added to each well, and the plate was incubated at room temperature for 1 h. Subsequently, 100 μL diluted HRP conjugated antibody was added to each well, and the plate was incubated at room temperature for an additional 1 h. Then 100 μL TMB Substrate Solution was added to each well, and the plate was incubated at room temperature for 15 min. Finally, 100 μL Stop Solution was added, and the plate was read within 5 min using a Multiskan™ GO plate reader at 450nm.

Localization of p53 protein in cells detected by immunofluorescence

The cellular distribution of p53 was determined by immunofluorescence. Cells (5×10^5/per well) were seeded in a 6-well plate with a sterilized coverslip at the bottom of each well. Cells were fixed with 4% paraformaldehyde for 15 min and subject to permeabilization using 0.5% Triton X-100 for 20 min. Subsequently, cells were incubated with goat serum for 1 h at 37 °C and a rabbit anti-p53 polyclonal antibody (Proteintech Group, Wuhan, China) at 4 °C overnight. Cells were washed and incubated with a Cy3-conjugated Goat Anti-rabbit IgG (H+L) for 1 h at room temperature. Cells were washed for three times in the dark and incubated with 4′,6-diamidino-2-phenylindole (DAPI) at room temperature for 10 min. Finally, the coverslip was sealed to a slide with an anti-fluorescence quenching agent, and cells were subject to imaging under a fluorescent microscope.

Detection of p53 mutation by DNA sequencing

Genomic DNA of HaCaT and HaCaT-T cells was extracted using Animal Genomic DNA Kit (TsingKe Biotech, China). Exons 5–9 of the p53 gene were amplified by PCR. The sequences of the primers are listed in Supplementary Table 2. PCR was performed under the

conditions: 94 °C for 3 min, 1 cycle, denaturation at 94 °C for 30 s, annealing at 58 °C for 3 s, extension at 72 °C for 1 min, 35 cycles. The PCR products of p53 gene in HaCaT and HaCaT-T cells were separated by gel electrophoresis in a 3% low melting agarose gel with EtBr. Subsequently, the PCR products were extracted from the gel, which was melted at 50 °C. The PCR products were reamplified under the same PCR conditions. The PCR products were then cloned into pTZ57R/T vector using InsTAclone PCR Cloning Kit (Thermo Scientific, Canada) and subject to DNA sequencing at the TsingKe Biotech Inc (Beijing, China).

Measurement of the level of m^{6}A in a specific mRNA by m^{6}A RNA immunoprecipitation assay (MeRIP)

The m^{6}A levels in the mRNA of the p53, PRDM2, MDM2, and YY1 gene were determined using Magna MeRIP™ m^{6}A Kit (A&D Technology Corporation, Beijing, China). Total RNA was extracted and analyzed as described above. mRNA was purified from total RNA using the Oligotex mRNA Kits (QIAGEN Group Inc., USA), and fragmented into 100 bp or smaller fragments. These fragmented mRNAs were further purified using miRcute miRNA isolation kit (Tiangen Biotech, Beijing Co., Ltd, China). Fragmented mRNAs were transferred into a new microcentrifuge tube followed by magnetic immunoprecipitation with m^{6}A monoclonal antibody. Briefly, MeRIP reaction mixture was incubated with an anti-m^{6}A antibody attached to magnetic beads for 2 h at 4 °C. The level of m^{6}A in the antibody-precipitated RNA fragments was determined by RT-qPCR. The levels of m^{6}A in the indicated genes were normalized to that of the internal control, GAPDH.

Bioinformatics analysis

Differentially expressed genes between HaCaT cells and HaCaT cells through chronic exposure to low concentrations of arsenite were obtained by GSE97303 [13]. The correlation among these differentially expressed genes, p53, and m^{6}A-regulating proteins was analyzed by STRIGN (https://string-db.org/). The sites of m^{6}A in mRNA were determined by analyzing m^{6}AVAR database (http://m6avar.renlab.org/index.html) [14] An analysis of the gene expression in skin cutaneous melanoma (SKCM) and its tumor purity, i.e., the percentage of cancer cells in total cells of tumor tissue, was performed using LINKEDOMICS (http://www.linkedomics.org/admin.php). The correlation of the gene expression with SKCM stage and prognosis was analyzed using GEPIA (http://gepia.cancer-pku.cn/index.html). The data of the gene expression in the cells and animals that were exposed to arsenic were obtained from GEO database (GSE47047, GSE97303, GSE103873, GSE2187, GSE33520, GSE36684, and GSE21193). Mutation and gene network analysis was performed using CBIOPORTAL (https://www.cbioportal.org/) and GENEMANIA (https://genemania.org/). The m^{6}A peaks on the PRDM2, MDM2, and YY1 mRNA were analyzed using CVm6A (http://gb.whu.edu.cn:8080/CVm6A).

Statistical analysis

All results were illustrated as mean ± standard error of the mean (SEM). A statistical significance was detected using Student's t-test or one-way analysis of variance (ANOVA) with SPSS 19.0 (SPSS Inc., Chicago, IL, USA). Bar charts and heat maps were created

using the GraphPad Prism 7.0 software. The interactive reticular chart was obtained by Cytoscape [15]. $P < 0.05$ was designated as a statistical difference.

Data availability

The source data for Figs. 1–6 are provided in Supplementary Table 1–5. The source data for Supplementary Figs. 1–6 are provided in Supplementary Table 6. The source data for p53 sequence are provided in the Supplementary p53 sequence.

Results

The level of m^{6}A is increased in arsenite-transformed human keratinocytes, HaCaT-T cells

To determine if the level of m^{6}A may be altered in arsenite-transformed human keratinocytes, we initially established an arsenite-transformed human keratinocyte line by chronically exposing human HaCaT keratinocytes to 1 μM arsenite for 5 months (50 passages). The transformed cell line was designated as HaCaT-T cells. We then characterized the transformation phenotypes of HaCaT-T cells. Compared with HaCaT cells (passed for 50 passages without arsenic exposure), HaCaT-T cells exhibited increased cell proliferation with a higher cell proliferation percentage than HaCaT cells at the time points of 48 h - 96 h (Fig. 1a). Also, HaCaT-T cells exhibited a significantly increased capacity of forming cell clones compared with HaCaT cells in both soft agar and 12-well plates (Fig. 1b and 1c). The results indicate that HaCaT-T cells were successfully transformed by chronic arsenite exposure.

To further determine the changes in the level of m^{6}A during arsenite-induced transformation, we measured the level of m^{6}A in HaCaT cells that were chronically exposed to a low dose of arsenite (1 μM). We found that the level of m^{6}A was significantly increased in arsenite-treated HaCaT cells at 30 and 50 passages (Fig. 1d). Since the level and function of m^{6}A are modulated by m^{6}A methyltransferases, demethylases, and m^{6}A readers [16–18], we further examined the expression levels of the m^{6}A-regulatory proteins in the arsenite-treated HaCaT cells at different passage numbers (Fig. 1e and 1f). We found that the expression of the m^{6}A methyltransferases, METTL3, METTL14, WTAP, KIAA1429, and the m^{6}A reader, YTHDF1 was increased in arsenite-treated HaCaT cells compared with the untreated HaCaT cells (Fig. 1e). Along with the increasing passage numbers, the expression of the proteins increased (Fig. 1f). In contrast, the demethylase of m^{6}A, FTO was decreased in the arsenite-treated cells at passage 30–50 (Fig. 1e and 1f). Our results are consistent with those from our bioinformatics analysis of the dataset from the TCGA database showing that the mRNA levels of METTL3, METTL14, KIAA1429, YTHDF1, and YTHDF2 are all positively associated with the tumor purity of SKCM (Supplementary Fig. 1a). In addition, a higher level of METTL3 and WTAP in the patients of SKCM of stage I-IV than that in stage 0 was detected (Supplementary Fig. 1b). All these results suggest that an increased level of m^{6}A induced by arsenite is associated with human keratinocyte transformation and skin cancer. Thus, it is possible that m^{6}A level in the cells may be altered by the aberrant expressions of m^{6}A methyltransferases, demethylases, and readers induced by arsenite resulting in keratinocyte transformation.

m^{6}A mediates the `migration and apoptosis of arsenite-transformed keratinocytes, HaCaT-T cells

To further determine the effects of m^{6}A methylation on arsenite-induced transformation, we examined the viability, migration, and apoptosis of HaCaT-T cells under the downregulation of m^{6}A by knocking down METTL3 using siRNAs (Fig. 2). We initially validated knockdown of METTL3 and the reduction of m^{6}A in HaCaT-T cells. As shown in Fig. 2a and 2b, knockdown of METTL3 significantly reduced its mRNA and protein levels in HaCaT cells and HaCaT-T cells (Fig. 2a and 2b). Consequently, the m^{6}A level in total RNA was significantly decreased compared with the HaCaT-T cells without or with scrambled siRNA (siControl) (Fig. 2c). However, the m^{6}A level in HaCaT cells was not altered by the knockdown of the methyltransferase (Fig. 2c). The results showed that METTL3 knockdown specifically reduced the level of METTL3 and m^{6}A in HaCaT-T cells. We then determined if this further affected the sensitivity of HaCaT-T cells to arsenite (Fig. 2d). We found that arsenite was more effective in reducing the viability of HaCaT-T cells with siMETTL3 than that of HaCaT-T cells without the siRNAs and the siControl (Fig. 2d). Next, we examined if METTL3 knockdown facilitated cell death through apoptosis induced by the cellular exposure to10 μM arsenite for 24 h (Fig. 2e). Indeed, we found that METTL3 knockdown resulted in a higher apoptosis rate in HaCaT-T cells than HaCaT-T cells and the siControl (Fig. 2e). The apoptosis rate was comparable to that of HaCaT with or without siRNAs (Fig. 2e, the bar chart). Finally, we examined the effects of METTL3 knockdown on the migration HaCaT-T cells using the wound-healing assay. The results revealed that HaCaT-T cell migration was significantly inhibited by METTL3 knockdown compared with the control cells (Fig. 2f). The results are consistent with those from our analysis of GEO database demonstrating that chronic arsenic exposure increased the expression of other m^{6}A methyltransferases, METTL3, METTL14, WTAP, KIAA1429, and the m^{6}A reader, YTHDF1 and decreased the expression of m^{6}A demethylase, FTO in several cell lines and animal models (Supplementary Fig. 2). This further indicates a possible role of m^{6}A in arsenite-induced cell transformation.

m^{6}A attenuates p53 activation to mediate arsenite-induced transformation.

Since m^{6}A is associated with p53 function [8–10], we further hypothesize that m^{6}A mediates arsenite-induced transformation by regulating the expression and activation of p53. To test this possibility, we initially determined if the mutations of p53 can be involved in arsenite-induced keratinocyte transformation, we sequenced a segment in the p53 encoding region of HaCaT and HaCaT-T cells (exons 5–9, commonly mutated regions in cancers [19]) (Fig. 3a). We failed to detect any mutations and differences in the sequence of the regions between HaCaT and HaCaT-T cells (Fig. 3a). The results are consistent with those from our bioinformatics analysis of the TCGA database showing that p53 mutations did not affect the survival of SKCM patients (Supplementary Fig. 3a) and are not associated with the expressions of m^{6}A-related proteins in SKCM tissue (Supplementary Fig. 3b). This further suggests that p53 mutations were not involved in m^{6}A-mediated HaCaT transformation induced by arsenite.

To further determine if m^{6}A can affect the expression level of p53, we examined the expression of p53 in HaCaT and HaCaT-T cells with METTL3 knockdown (Fig. 3b and 3c).

We found that the mRNA level of p53 in these cells was not significantly altered by the METTL3 knockdown. Instead, the gene knockdown did not result in a higher p53 protein level in HaCaT-T cells than HaCaT cells (Fig. 3c), suggesting that m^6A mediated arsenite-induced cell transformation independent of p53 gene expression. This is further supported by our analysis of the GEO database showing that the mRNA level of p53 in HaCaT, prostate epithelial cells, and rat liver tissue was not significantly altered by arsenite (Supplementary Fig. 3c).

We then asked if m^6A can mediate arsenite-induced keratinocyte transformation by modulating the activation of p53. We found that p53 activity was significantly decreased in HaCaT-T cells, and this was reversed by knockdown of METTL3 in HaCaT-T cells (Fig. 3d). Since p53 activity can also be determined by the expression of the p53 target genes, the cellular localization and posttranslational modifications of p53 protein [20–22], we then examined the expression of three p53 target genes, CDKN1A, RRM2B, SUSD6 (KIAA0247) in HaCaT and HaCaT-T cells. These genes are involved in cell cycle arrest in G1 phase [23], DNA repair and mtDNA synthesis [24], suppression of cell proliferation, and angiogenesis and promotion of apoptosis [25]. We found that all the p53 target genes were significantly lower in HaCaT-T cells than HaCaT cells (Fig. 3e–3g). The suppression of the gene expression in HaCaT-T cells was relieved by knockdown of METTL3 (Fig. 3e–3g). In consistency with our experimental results, the results from our bioinformatics analysis showed that the expression of RRM2B, CDKN1A and SUSD6 was also decreased in HaCaT cells and mice (Supplementary Fig. 4a), SKCM cancer tissue (Supplementary Fig. 4b), and patients (Supplementary Fig. 4c and 4d). All these results suggest that m^6A mediated arsenite-induced keratinocyte transformation by reducing the transcriptional activity of p53.

We then determined if m^6A can promote the nuclear export of p53 protein to inactivate the protein by altering its cellular compartmentalization [11]. We found that in HaCaT-T cells, p53 nuclear localization was significantly reduced along with an increased amount of cytoplasmic staining of p53, and this was significantly reversed by knockdown of METTL3 in HaCaT-T cells (Fig. 4a). To further determine the roles of m^6A on p53 activation in mediating arsenite-induced HaCaT cell transformation, we also measured the level of p53 phosphorylation and acetylation at different amino acids (Fig. 4b). We found that the phosphorylation of p53 at Ser15 that is critical for p53 stabilization [26] was increased in HaCaT-T cells (Fig. 4b). Also, we found that p53 phosphorylation at Ser392 that is essential for the stability of p53 tetramerization domain and its DNA binding [27,28], was significantly decreased in HaCaT-T cells (Fig. 4b), and p53 acetylation at Lys382 that is critical for p53 activation [29] was reduced in the cells (Fig. 4b). Further, we found that knockdown of METTL3 significantly increased the phosphorylation at Ser392 and acetylation at Lys382 in HaCaT-T cells (Fig. 4b). However, we found that elevated phosphorylation at Ser15 was not ameliorated in HaCaT-T cells with siMETTL3 (Fig. 4b). The results suggest that m^6A mediated arsenite-induced human keratinocyte transformation by suppressing p53 activation rather than affecting p53 gene expression.

m^{6}A modulates the expression of p53 activation regulators to mediate arsenite-induced keratinocyte transformation

To further explore the mechanisms by which m^{6}A inhibited p53 activation, we initially conducted a bioinformatics analysis of the published data (GSE 97303) to identify the genes that are associated with m^{6}A and p53 in HaCaT cells that were chronically exposed to a low dose of arsenite. We found that the PRDM2, MDM2, YY1, ESR2, TCF7L2, FUS, RNPS1, and RQCD1 gene that are involved in arsenite-induced transformation, were associated with m^{6}A and p53 (Fig. 5a, boxes in pink; Supplementary Table 3). Among these genes, the PRDM2, MDM2, and YY1 gene, which are the regulators of p53 activation [30–32] have the m^{6}A sites in their mRNAs, which have been identified by the miCLIP/PA-m^{6}A-seq or MeRIP-Seq experiments (Fig. 5b; Supplementary Table 4). Our experimental results further demonstrated that the mRNA and protein levels of PRDM2 that upregulates p53 activation [30] were decreased in HaCaT-T cells compared to HaCaT cells (Fig. 5c and 5f). On the other hand, we found that in HaCaT-T cells, the mRNA and protein levels of MDM2, an inhibitor of p53 activation [31,33,34] and YY1, a negative regulator of p53 [32] were increased (Fig. 5d–5f). The changes of PRDM2, MDM2, and YY1 are consistent with p53 inactivation in HaCaT-T cells. Moreover, our bioinformatics analysis found that the expression of PRDM2 was also decreased in arsenite-transformed malignant prostate epithelial cells, and the expression of YY1 was increased in human bronchial epithelial cell line and mice that were chronically exposed to arsenite (Supplementary Fig. 5a). Furthermore, we found that the mRNA level of PRDM2 was negatively correlated to SKCM tumor purity, whereas the mRNA level of MDM2 and YY1 was positively correlated to SKCM tumor purity (Supplementary Fig. 5b). Our bioinformatics analysis also showed that the YY1 RNA level was elevated in SKCM patients at stage I-IV (Supplementary Fig. 5c) and served as the core of the network, including MDM2 and p53 (Supplementary Fig. 5d). All of these results indicate that the p53 activation regulators affected by m^{6}A were involved in arsenite-induced transformation of human keratinocytes.

To further determine if the expression of PRDM2, MDM2, and YY1 can be modulated by elevated m^{6}A, we performed an additional bioinformatic analysis of the dataset from the TCGA database, the results showed that the mRNA level of these p53 regulators was significantly correlated to that of METTL3 gene in SKCM patient tissue (Supplementary Fig. 6a) suggesting that m^{6}A stimulated the expression of the p53 activation regulators in the patient tissue. To determine if m^{6}A is involved in the arsenite-induced keratinocyte transformation through the regulation of the expression of the PRDM2, MDM2, and YY1 gene, we then examined if knockdown of METTL3 can alter the expression of the genes in HaCaT-T cells. We found that knockdown of METTL3 by METTL3 siRNA (siMETTL3) in HaCaT-T cells partially relieved the inhibition of the p53 positive regulator, PRDM2, but decreased the level of the overexpression of the p53 suppressor, MDM2 and YY1 in the cells (Fig 5c–5f). Furthermore, since our bioinformatic analysis of the m^{6}A database (CVm6A) showed m^{6}A peaks on the mRNA of the PRDM2, MDM2, and YY1 (Supplementary Fig. 6b), we then determined the m^{6}A level in p53 mRNA in HaCaT and HaCaT-T cells using MeRIP. The results showed that although the m^{6}A level in p53 mRNA was not significantly altered in HaCaT-T cells (Fig. 6a), the m^{6}A levels on the mRNA of the PRDM2, MDM2, and YY1 were significantly increased in HaCaT-T cells compared with HaCaT cells (Fig.

6b–6d). These results suggested that elevated m^{6}A regulated p53 activation by mediating the regulators of p53 activation in arsenite-induced human keratinocyte transformation.

To explore the mechanisms by which m^{6}A modulates the regulators of p53 activation in HaCaT-T cells, we knocked down YTHDF1 and YTHDF2 in the cells using siRNAs. We found that knockdown of YTHDF1 that promotes translation of m^{6}A-methylated transcripts decreased both the mRNA and protein levels of MDM2 and YY1 (Fig. 6e and 6f). However, knockdown of YTHDF2 that promotes the decay of m^{6}A-methylated transcripts, elevated the mRNA and protein levels of PRDM2 in the cells (Fig. 6e and 6g). The results indicated that decreased YTHDF1 suppressed the expression of MDM2 and YY1, whereas decreased YTHDF2 increased the level of PRDM2 mRNA and protein. Taken together, both our bioinformatics analysis and experimental results revealed that m^{6}A resulted in p53 inactivation by modulating p53 activation regulators in arsenite-transformed human keratinocytes.

Discussion

In this study, we discovered that in the arsenite-transformed keratinocytes HaCaT-T cells, m^{6}A methyltransferases, METTL3, METTL14, WTAP, and KIAA1429 were upregulated, whereas the m^{6}A demethylase, FTO was downregulated (Figure 1). We demonstrated that the cellular level of m^{6}A was increased (Figure 1d), and this, in turn, suppressed the expression of the upregulator of p53 activation, PRDM2, and stimulated the expression of the downregulators of p53 activation, MDM2, and YY1 (Figure 5–6). Consequently, this led to p53 inactivation and cellular transformation of human keratinocytes. Our results suggest that m^{6}A mediated arsenite-induced transformation of keratinocytes through suppression of p53 activation. Our results further support a model during which arsenite stimulates the RNA methyltransferases and cofactors, METTL3, METTL14, KIAA1429, and WTAP (Fig. 7). This induces the production of m^{6}A in the mRNAs of PRDM2 (Fig. 7, pathway 1) or that of m^{6}A in the mRNAs of MDM2 and YY1 (Fig. 7, pathway 2). Subsequently, m^{6}A in the mRNAs of PRDM2 is bound by YTHDF2, whereas m^{6}A in the mRNAs of MDM2 and YY1 is bound by YTHDF1 resulting in the degradation of PRDM2 mRNA (Fig. 7, pathway 1) and stabilization of the mRNA of MDM2 and YY1 (Fig. 7, pathway 2). Consequently, this increases p53 nuclear export and decreases p53 phosphorylation and acetylation at Ser392 and Ser382, respectively, leading to p53 inactivation and keratinocyte transformation (Fig. 7).

Among several proteins that have been identified in the m^{6}A “writer” complex, including METTL3, METTL14, WTAP, and KIAA1429 [16–18], METTL3 is the one that plays a key role in generating m^{6}A. This is because genetic depletion of METTL3 in plants, yeast, and mammalian cells results in nearly complete loss of m^{6}A in polyadenylated RNA [34–36]. However, other members in the complex do not possess catalytic activity and are only involved in stabilizing the assembly of the complex and recruitment of METTL3 to its target mRNAs in specific subcellular locations [37]. Also, METTL3 is overexpressed in different types of cells, including HaCaT cells and animals that are exposed to arsenite based on our experimental results (Fig. 1e and 1f) and our bioinformatics analysis of the published databases (Supplementary Fig. 2). Moreover, our analysis of the TCGA database showed

that the mRNA level of METTL3 is positively associated with tumor purity of skin cutaneous melanoma (Supplementary Fig. 1a), and a higher level of METTL3 was detected in the patients of skin cutaneous melanoma of stage I-IV than those in stage 0 (Supplementary Fig. 1b). These results indicate a crucial role of METTL3 in m^6A production and regulation and arsenite-induced skin carcinogenesis. Therefore, we decided to knockdown METTL3 in our experiments. Interestingly, we did not observe a significant change in m^6A level in HaCaT cells with knockdown of METTL3. This may be due to a low m^6A level in HaCaT cells. It has been reported that approximately 0.1–0.4% of adenosine nucleotides in mammalian RNAs are chemically modified [38]. In our experiments, m^6A level was only about 0.275% in HaCaT cells. Our results showed that knockdown of METTL3 decreased the m^6A level in HaCaT cells from 0.275% to 0.255%. Such a small change of the m^6A level was not statistically significant.

Previous studies have focused on the mechanisms underlying arsenite carcinogenesis through aberrant gene expression and mutations, as well as altered functions of proteins. Here, we proposed a new mechanism by which arsenite induces cell transformation associated with skin cancer through m^6A. A recent study from our group has provided the first evidence that m^6A is involved in arsenite-induced cell transformation [4]. In this study, we further demonstrated that m^6A mediated arsenite-induced cell transformation by inhibiting p53 activation rather than by altering p53 expression (Fig. 3–4). However, our experiments have several limitations. First, in our studies, the wound-healing assay was used to determine cell invasion. The results from the assay may not completely match the results from the cell-transformation experiments. Second, since we used transient transfection of short interfering RNA (siRNAs) to knockdown genes, we could not detect the effects of siRNA on HaCaT cells using the soft agar clone formation assay and plate colony formation assay. This is because both assays require the growth of cells for at least 10 days. Thus, we only detected the effects of transient siRNA transfection on the transformation of HaCaT cells using cell viability assay, wound-healing assay, and cell apoptosis, which only require short period of time (24 h).

In this study, we tested p53 activation by determining p53 activity, p53 phosphorylation and acetylation, p53 localization, the expression of p53 target genes and p53 regulators, and apoptosis to demonstrate p53 activation. p53 activity was determined based on the principle that p53 protein binds to a consensus p53-binding site and activates the expression of downstream genes [21,22] using a commercial p53 Activity Assay kit. However, it should be noted that the activation of p53 and the regulation of its downstream targets are also mediated by p53 posttranslational modifications and modulated by p53 regulators [39]. Our approaches not only have demonstrated the p53 activation from different aspects but also are beneficial for the future research on understanding the mechanisms of p53 inactivation mediated by m^6A in arsenite-induced cell transformation.

There has been a controversy regarding whether chronic arsenite exposure can lead to carcinogenesis by inducing p53 mutations based on population-based studies [40–42]. This is because the results from the population-based studies are usually affected by a variety of confounding factors, which can introduce the bias to the results of p53 mutational studies, especially those from the human population that was chronically exposed to low doses of

arsenite. In addition, the population-based analysis has a limitation for detecting precise alterations of p53 in cells. Using cell models, we were able to show that chronic arsenite exposure at low doses did not induce the p53 gene mutations in its exons 5–9 [19,438](Fig. 3a). The results are consistent with a report showing that no p53 mutations in exons 5–8 are detected in rats that are exposed to the metabolite of arsenite, dimethylarsinic acid [44] Thus, our results suggest that it is unlikely that p53 mutations and aberrant expression were involved in arsenite-induced human keratinocytes transformation that was mediated by m^6A. Instead, it was the suppression of p53 activation that mediated arsenite-induced human keratinocyte transformation and carcinogenesis. This is also supported by the studies that have shown that arsenite suppresses p53 activation by decreasing p53 acetylation and phosphorylation[13], inducing p53 poly(ADP-ribosyl)ation [45], and inhibiting the DNA binding activity of p53 and its target gene p21 expression [46]. Furthermore, it has been found that microRNA, miR-410, −548ac, and −548a-3p, and p53 regulators, HMGB1 and MDM2 can also be involved in the suppression of p53 activation induced by arsenite in cellular transformation and carcinogenesis [13,47]. However, our results cannot exclude a possibility that m^6A transcripts in p53 may facilitate the selection of a mutated codon in the other encoding regions of the protein through m^6A in TP53 codon RNA transcripts that promote the selection of m^6A-R273H pre-mRNA for splicing producing the mutant protein in cancer cells [48]. Thus, our study revealed the m^6A-mediated mechanism underlying arsenite-induced human keratinocyte transformation, shedding light on the complex mechanisms by which arsenite induces alterations of p53 activation in cell transformation and carcinogenesis.

It is suggested that there is a significant association between cutaneous melanoma and exposure to arsenical pesticides [49]. It is also found that the mortality rate of melanoma is significantly increased in the population that was occupationally exposed to arsenic [50]. Moreover, the increased mortality of skin cancer, including melanoma is higher than the predicted rate resulting from aging suggesting that the increased mortality results from environmental exposure such as arsenic exposure [51]. Further, since both melanocytes and keratinocytes are target cells in the skin and share the same mechanism by which arsenic inhibits DNA repair, chronic arsenic exposure may promote the accumulation of unrepaired DNA damage in melanocytes causing melanoma [52]. Thus, all these studies point to a strong correlation between skin cutaneous melanoma (SKCM) and arsenic exposure supporting a notion that arsenite exposure is a risk factor of SKCM. Our bioinformatic analysis of SKCM from several human studies further demonstrated that m^6A methyltransferases and readers were associated with the development of SKCM, suggesting an important role of m^6A in mediating the development of skin cancer. Our bioinformatics analysis of p53 mutation and expression, its target genes, and regulators in SKCM further indicated that p53 inactivation played a crucial role in the development of skin cancer. Our bioinformatics analysis of the co-expression of both m^6A methyltransferases and p53 regulators in SKCM tissue also indicated a correlation between m^6A and p53 in skin cancer. Thus, our bioinformatics analysis results support the conclusions from our experimental results.

Since its discovery in 2012 [8], the cellular function of m^6A and its regulation have been studied extensively, and its “writer”, “eraser”, and “reader” have been identified, and its roles in various biological processes and the development of diseases have been reported [17,53]. Recent studies have also demonstrated that m^6A serves as a beacon for the recruitment

of a repair DNA polymerase to UV damage sites [54] and is involved in neurite outgrowth recovery in mouse neurons that are exposed to arsenite [55] indicating its important role in the arsenite-driven hormesis on cytotoxicity [5]. Further, our bioinformatic analysis on the network of m^6A- and p53-related genes in this study demonstrated that one function of the m^6A- and p53-related genes in the network is to mediate cellular response to hypoxia and oxygen levels (Supplementary Fig. 6c). This is also consistent with the other study [55] that suggests that there is an association between m^6A and oxidative stress. This is further supported by our recent findings showing that m^6A is associated with oxidative stress in arsenite-driven hormesis [5], and arsenite-induced oxidative stress increases the levels of m^6A [6]. All these studies suggest the critical roles of m^6A in mediating and modulating geno- and cytotoxicity of environmental toxicants including arsenite. The roles of m^6A in oxidative stress, as well as the toxic effects of other environmental toxicants and their underlying mechanisms, need to be further elucidated in the future.

Supplementary Material

Refer to Web version on PubMed Central for supplementary material.

Acknowledgments

We appreciate the technical support of the Public Health and Preventive Medicine Provincial Experiment Teaching Center at Sichuan University and Food Safety Monitoring and Risk Assessment Key Laboratory of Sichuan Province.

Funding

Funding: This work was supported by the grant from the National Science Foundation of China (No. 81773380). Y. Lai and Y. Liu are supported by NIHR01ES023569.

Abbreviations

m^6A	N^6-methyladenosine
IARC	International Agency for Research on Cancer
PBS	hosphate-buffered saline
FITC	fluorescein isothiocyanate
PI	propidium iodide
DAPI	4′,6-diamidino-2-phenylindole
TCGA	The Cancer Genome Atlas
SKCM	skin cutaneous melanoma
SEM	standard error of the mean
METTL3	methyltransferase-like 3
METTL14	methyltransferase-like 14

WTAP	Wilms tumor 1-associated protein
VIRMA/KIAA1429	via like m^6A methyltransferase associated
FTO	fat mass and obesity-associated protein
YTHDF1	YTH N^6-methyladenosine RNA binding protein 1
YTHDF1	YTH N^6-methyladenosine RNA binding protein 2
CDKN1A	cyclin dependent kinase inhibitor 1A
RRM2B	ribonucleotide reductase regulatory TP53 inducible subunit M2B
SUSD6/ KIAA0247	sushi domain containing 6
PRDM2	PR/SET domain 2
MDM2	murine double minute 2
YY1	Yin Yang-1

References

1. Sen P, Biswas T Arsenic: the largest mass poisoning of a population in history. BMJ 346, f3625, doi: 10.1136/bmj.f3625 (2013). [PubMed: 23741031]
2. Navas-Acien A, Nachman KE. Public health responses to arsenic in rice and other foods. JAMA Intern Med 173(15), 1395–1396, doi: 10.1001/jamainternmed.2013.6405 (2013). [PubMed: 23700006]
3. Humans, I. W. G. o. t. E. o. C. R. t. Arsenic, metals, fibres, and dusts. IARC Monogr Eval Carcinog Risks Hum 100, 11–465 (2012). [PubMed: 23189751]
4. Gu S, Sun D, Dai H & Zhang Z N^6-methyladenosine mediates the cellular proliferation and apoptosis via microRNAs in arsenite-transformed cells. Toxicol Lett 292, 1–11, doi:10.1016/j.toxlet.2018.04.018 (2018). [PubMed: 29680375]
5. Chen H, Zhao T, Sun D, Wu M & Zhang Z Changes of RNA N6-methyladenosine in the hormesis effect induced by arsenite on human keratinocyte cells. Toxicol In Vitro 56, 84–92, doi: 10.1016/j.tiv.2019.01.010 (2019). [PubMed: 30654086]
6. Zhao T, Li X, Sun D & Zhang Z Oxidative stress: One potential factor for arsenite-induced increase of N6-methyladenosine in human keratinocytes. Environ Toxicol Pharmacol 69, 95–103, doi:10.1016/j.etap.2019.04.005 (2019). [PubMed: 31004932]
7. Bai L et al. m6A demethylase FTO regulates dopaminergic neurotransmission deficits caused by arsenite. Toxicol Sci, doi:10.1093/toxsci/kfy172 (2018).
8. Dominissini D et al. Topology of the human and mouse m6A RNA methylomes revealed by m6A-seq. Nature 485, 201–206, doi:10.1038/nature11112 (2012). [PubMed: 22575960]
9. Kwok CT, Marshall AD, Rasko JE & Wong JJ Genetic alterations of m6A regulators predict poorer survival in acute myeloid leukemia. J Hematol Oncol 10, 39–45, doi: 10.1186/s13045-017-0410-6 (2017). [PubMed: 28153030]
10. Zheng G et al. ALKBH5 is a mammalian RNA demethylase that impacts RNA metabolism and mouse fertility. Mol Cell 49, 18–29, doi:10.1016/j.molcel.2012.10.015 (2013). [PubMed: 23177736]
11. Huang Y et al. Induction of cytoplasmic accumulation of p53: a mechanism for low levels of arsenic exposure to predispose cells for malignant transformation. Cancer Res 68, 9131–9136, doi:10.1158/0008-5472.CAN-08-3025 (2008). [PubMed: 19010883]

12. Zhou Y et al. Low dose arsenite confers resistance to UV induced apoptosis via p53-MDM2 pathway in ketatinocytes. Oncogenesis 6, e370, doi:10.1038/oncsis.2017.67 (2017). [PubMed: 28785074]
13. Al-Eryani L et al. Differentially Expressed mRNA Targets of Differentially Expressed miRNAs Predict Changes in the TP53 Axis and Carcinogenesis-Related Pathways in Human Keratinocytes Chronically Exposed to Arsenic. Toxicol Sci 162, 645–654, doi:10.1093/toxsci/kfx292 (2018). [PubMed: 29319823]
14. Zheng Y et al. m6AVar: a database of functional variants involved in m6A modification. Nucleic Acids Res 46, D139–D145, doi:10.1093/nar/gkx895 (2018). [PubMed: 29036329]
15. Shannon P et al. Cytoscape: a software environment for integrated models of biomolecular interaction networks. Genome Res 13, 2498–2504, doi: 10.1101/gr.1239303 (2003). [PubMed: 14597658]
16. Niu Y et al. N6-methyl-adenosine (m6A) in RNA: an old modification with a novel epigenetic function. Genomics Proteomics Bioinformatics 11, 8–17, doi:10.1016/j.gpb.2012.12.002 (2013). [PubMed: 23453015]
17. Bi Z et al. A dynamic reversible RNA N6 -methyladenosine modification: current status and perspectives. J Cell Physiol, doi:10.1002/jcp.28014 (2019).
18. Pan Y, Ma P, Liu Y, Li W & Shu Y Multiple functions of m6A RNA methylation in cancer. J Hematol Oncol 11, 48, doi:10.1186/s13045-018-0590-8 (2018). [PubMed: 29587823]
19. Leroy B, Anderson M & Soussi T TP53 mutations in human cancer: database reassessment and prospects for the next decade. Hum Mutat 35, 672–688, doi:10.1002/humu.22552 (2014). [PubMed: 24665023]
20. Yamamoto S & Iwakuma T Regulators of Oncogenic Mutant TP53 Gain of Function. Cancers (Basel) 11, doi:10.3390/cancers11010004 (2018).
21. Raj N & Attardi LD The Transactivation Domains of the p53 Protein. Cold Spring Harb Perspect Med 7, doi:10.1101/cshperspect.a026047 (2017).
22. Saha T, Kar RK & Sa G Structural and sequential context of p53: A review of experimental and theoretical evidence. Prog Biophys Mol Biol 117, 250–263, doi:10.1016/j.pbiomolbio.2014.12.002 (2015). [PubMed: 25550083]
23. Georgakilas AG, Martin OA & Bonner WM p21: A Two-Faced Genome Guardian. Trends Mol Med 23, 310–319, doi:10.1016/j.molmed.2017.02.001 (2017). [PubMed: 28279624]
24. Pitceathly RD. et al. Adults with RRM2B-related mitochondrial disease have distinct clinical and molecular characteristics. Brain 135, 3392–3403, doi: 10.1093/brain/aws231. Epub 2012 Oct 29 (2012). [PubMed: 23107649]
25. Polato F et al. DRAGO (KIAA0247), a new DNA damage-responsive, p53-inducible gene that cooperates with p53 as oncosuppressor. [Corrected]. J Natl Cancer Inst 106, dju053, doi:10.1093/jnci/dju053 (2014). [PubMed: 24652652]
26. Yuan F et al. Up-regulation of Siah1 by ethanol triggers apoptosis in neural crest cells through p38 MAPK-mediated activation of p53 signaling pathway. Arch Toxicol 91, 775–784, doi: 10.1007/s00204-016-1746-3 (2017). [PubMed: 27270636]
27. Lagunas-Martinez A et al. MG132 plus apoptosis antigen-1 (APO-1) antibody cooperate to restore p53 activity inducing autophagy and p53-dependent apoptosis in HPV16 E6-expressing keratinocytes. Apoptosis 22, 27–40, doi:10.1007/s10495-016-1299-1 (2017). [PubMed: 27766434]
28. Ishak Gabra MB et al. IKKβ activates p53 to promote cancer cell adaptation to glutamine deprivation. Oncogenesis 7, 93, doi:10.1038/s41389-018-0104-0 (2018). [PubMed: 30478303]
29. Wu CE et al. Targeting negative regulation of p53 by MDM2 and WIP1 as a therapeutic strategy in cutaneous melanoma. Br J Cancer 118, 495–508, doi:10.1038/bjc.2017.433 (2018). [PubMed: 29235570]
30. Shadat NM et al. Retinoblastoma protein-interacting zinc finger 1 (RIZ1) regulates the proliferation of monocytic leukemia cells via activation of p53. Cancer Invest 28, 806–812, doi:10.3109/07357907.2010.494323 (2010). [PubMed: 20594067]
31. Tackmann NR & Zhang Y Mouse modelling of the MDM2/MDMX-p53 signalling axis. J Mol Cell Biol 9, 34–44, doi:10.1093/jmcb/mjx006 (2017). [PubMed: 28096294]

32. Inoue K, Fry EA & Frazier DP Transcription factors that interact with p53 and Mdm2. Int J Cancer 138, 1577–1585, doi:10.1002/ijc.29663 (2016). [PubMed: 26132471]
33. Wei J et al. Escape, or Vanish: Control the Fate of p53 through MDM2-Mediated Ubiquitination. Anticancer Agents Med Chem 16, 174–189, doi: 10.2174/1871520615666150907093358 (2015). [PubMed: 26343143]
34. Agarwala SD. et al. RNA methylation by the MIS complex regulates a cell fate decision in yeast. PLoS Genet 8, e1002732, doi: 10.1371/journal.pgen.1002732 (2012). [PubMed: 22685417]
35. Geula S et al. Stem cells. m6A mRNA methylation facilitates resolution of naive pluripotency toward differentiation. Science 347, 1002–1006, doi: 10.1126/science.1261417 (2015). [PubMed: 25569111]
36. Zhong S et al. MTA is an Arabidopsis messenger RNA adenosine methylase and interacts with a homolog of a sex-specific splicing factor. Plant Cell 20, 1278–1288, doi: 10.1105/tpc.108.058883 (2008). [PubMed: 18505803]
37. Vu LP. et al. The Biology of m6A RNA Methylation in Normal and Malignant Hematopoiesis. Cancer Discov 9(1), 25–33, doi: 10.1158/2159-8290.CD-18-0959 (2019). [PubMed: 30578356]
38. Wei CM. et al. Methylated nucleotides block 5′terminus of HeLa cell messenger RNA. Cell 4(4), 379–386, doi: 10.1016/0092-8674(75)90158-0 (1975). [PubMed: 164293]
39. Riley T et al. Transcriptional control of human p53-regulated genes. Nat Rev Mol Cell Biol 9(5), 402–412, doi: 10.1038/nrm2395 (2008). [PubMed: 18431400]
40. Kelsey KT et al. TP53 alterations and patterns of carcinogen exposure in a U.S. population-based study of bladder cancer. Int J Cancer 117, 370–375, doi:10.1002/ijc.21195 (2005). [PubMed: 15906354]
41. Zhang A et al. Unventilated indoor coal-fired stoves in Guizhou province, China: cellular and genetic damage in villagers exposed to arsenic in food and air. Environ Health Perspect 115, 653–658, doi:10.1289/ehp.9272 (2007). [PubMed: 17450239]
42. Moore LE et al. P53 alterations in bladder tumors from arsenic and tobacco exposed patients. Carcinogenesis 24, 1785–1791, doi:10.1093/carcin/bgg136 (2003). [PubMed: 12919957]
43. Bykov VJN, Eriksson SE, Bianchi J & Wiman KG Targeting mutant p53 for efficient cancer therapy. Nat Rev Cancer 18, 89–102, doi:10.1038/nrc.2017.109 (2018). [PubMed: 29242642]
44. Wei M et al. Carcinogenicity of dimethylarsinic acid in male F344 rats and genetic alterations in induced urinary bladder tumors. Carcinogenesis 23, 1387–1397, doi:10.1093/carcin/23.8.1387 (2002). [PubMed: 12151359]
45. Komissarova EV & Rossman TG Arsenite induced poly(ADP-ribosyl)ation of tumor suppressor P53 in human skin keratinocytes as a possible mechanism for carcinogenesis associated with arsenic exposure. Toxicol Appl Pharmacol 243, 399–404, doi:10.1016/j.taap.2009.12.014 (2010). [PubMed: 20036271]
46. Tang F et al. Arsenite inhibits p53 phosphorylation, DNA binding activity, and p53 target gene p21 expression in mouse epidermal JB6 cells. Mol Carcinog 45, 861–870, doi: 10.1002/mc.20245 (2006). [PubMed: 16739126]
47. Pant V & Lozano G Dissecting the p53-Mdm2 feedback loop in vivo: uncoupling the role in p53 stability and activity. Oncotarget 5, 1149–1156, doi:10.18632/oncotarget.1797 (2014). [PubMed: 24658419]
48. Uddin MB. et al. An N6-methyladenosine at the transited codon 273 of p53 pre-mRNA promotes the expression of R273H mutant protein and drug resistance of cancer cells. Biochem Pharmacol 160, 134–145, doi: 10.1016/j.bcp.2018.12.014. (2019). [PubMed: 30578766]
49. Dennis LK. et al. Pesticide use and cutaneous melanoma in pesticide applicators in the agricultural heath study. Environ Health Perspect 118(6), 812–817, doi: 10.1289/ehp.0901518. (2010). [PubMed: 20164001]
50. Gianicolo EAL. et al. Long-term effect of arsenic exposure: Results from an occupational cohort study. Am J Ind Med 62(2), 145–155, doi: 10.1002/ajim.22939. (2019). [PubMed: 30609098]
51. Alonso FT. et al. Increased skin cancer mortality in Chile beyond the effect of ageing: Temporal analysis 1990 to 2005. Acta Derm Venereol 90(2), 141–146, doi: 10.2340/00015555-0787. (2010). [PubMed: 20169296]

52. Cooper KL. et al. Melanocytes and keratinocytes have distinct and shared responses to ultraviolet radiation and arsenic. Toxicol Lett 224(3), 407–415, doi: 10.1016/j.toxlet.2013.11.010. (2013). [PubMed: 24270004]

53. Maity A & Das B N6-methyladenosine modification in mRNA: machinery, function and implications for health and diseases. FEBS J 283, 1607–1630, doi: 10.1111/febs.13614 (2016). [PubMed: 26645578]

54. Xiang Y et al. RNA m6A methylation regulates the ultraviolet-induced DNA damage response. Nature 543, 573–576, doi:10.1038/nature21671 (2017). [PubMed: 28297716]

55. Li M et al. Ythdf2-mediated m6A mRNA clearance modulates neural development in mice. Genome Biol 19, 69–85, doi:10.1186/s13059-018-1436-y (2018). [PubMed: 29855337]

Highlights

1. The level of m^6A is increased in arsenite-transformed human keratinocytes
2. m^6A mediates migration and apoptosis of arsenite-transformed keratinocytes
3. m^6A attenuates p53 activation instead of expression in arsenite-transformed cells
4. m^6A suppresses p53 by altering the expression of p53 activation regulators
5. m^6A writers, erasers, and readers mediates the function of m^6A on p53 inactivation

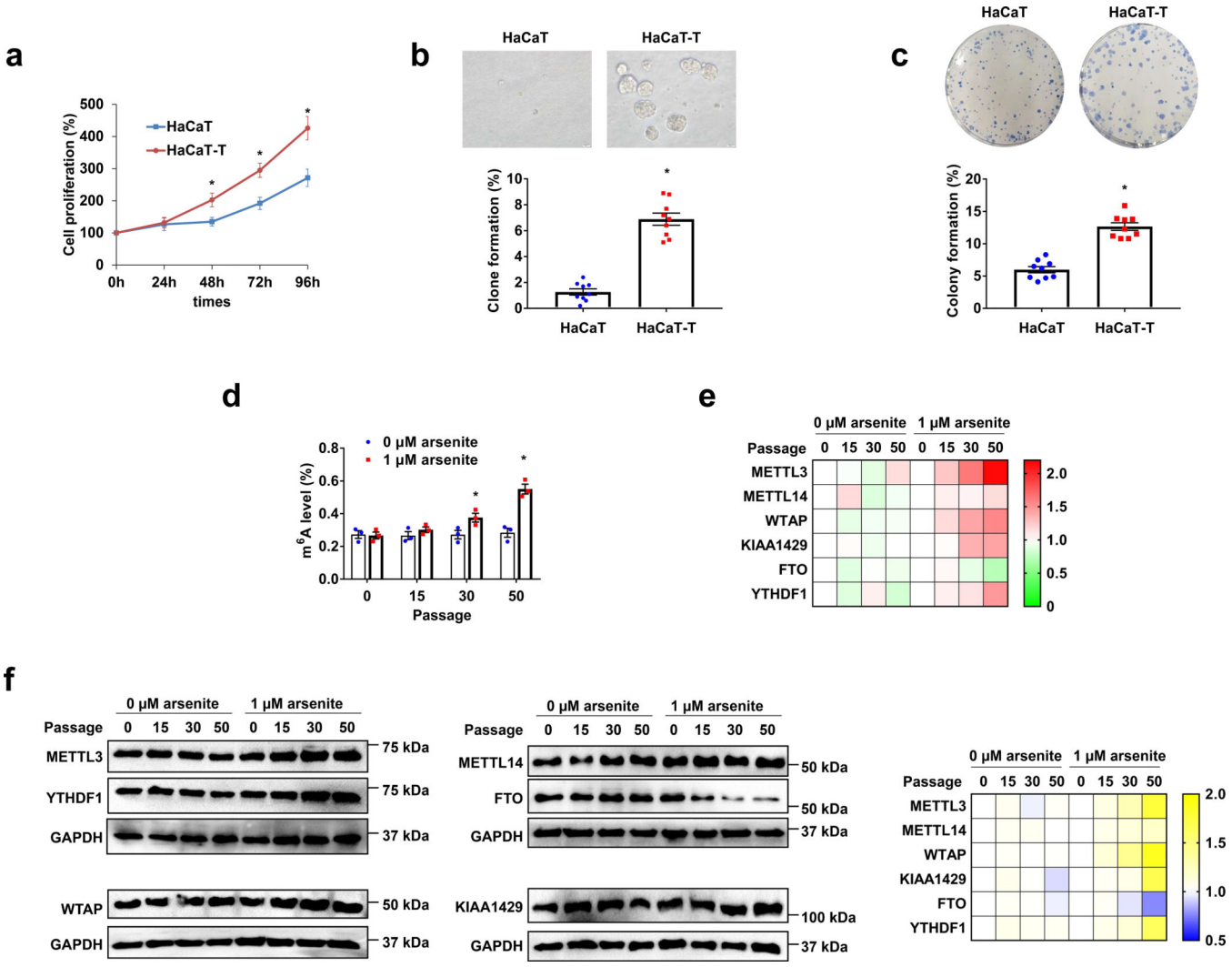

Fig. 1. m^{6}A level increases in arsenite-transformed human keratinocytes.

a, Cell proliferation of HaCaT and HaCaT-T cells was measured by MTT assay. **b**, Percentage of clone formation was calculated by soft agar clone formation assay in HaCaT and HaCaT-T cells (down). Representative images of HaCaT and HaCaT-T cells in soft agar clone formation assay observed with a microscope at 400× magnification (up). **c**, Percentage of colony formation was tested by plate colony formation assay in HaCaT and HaCaT-T cells (down). Representative images of HaCaT and HaCaT-T cells in plate colony formation (up). **d**, Total m^{6}A levels in HaCaT and HaCaT-T cells of 0, 15, 30, 50 passages were determined by EpiQuik m^{6}A RNA Methylation Quantification Kit. **e**, **f**, RT-qPCR testing the mRNA levels (**e**) and western blotting examining the protein levels (**f**) of m^{6}A regulating proteins (METTL3, METTL14, WTAP, KIAA1429, FTO, and YTHDF1) in HaCaT and HaCaT-T cells of 0, 15, 30, 50 passages are shown in heat maps. Representative images of immunoblot (f, left). For **a-f**, n = at least 3 biological replicates, error bars indicate mean ± SEM. The *P*-values were determined by two-tailed t-test. "*" indicates a significant difference compared to control group ($P < 0.05$).

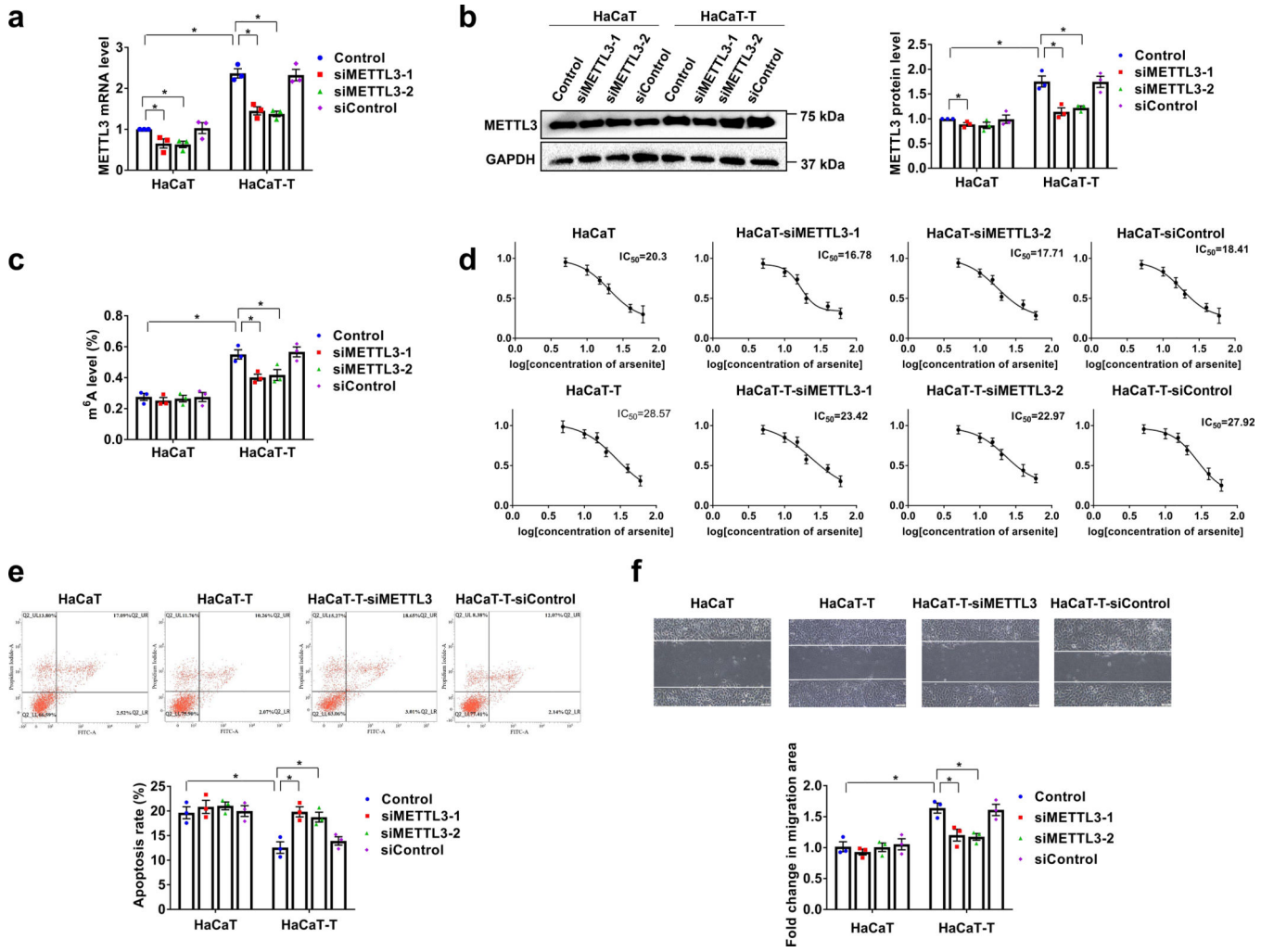

Fig. 2. m^{6}A mediates migration and apoptosis in arsenite-transformed keratinocytes.

a, **b**, The mRNA (**a**) and protein (**b**) levels of METTL3 in HaCaT and HaCaT-T cells with introduction of two siMETTL3 (siMETTL3–1 and siMETTL3–2) and siControl were tested by RT-qPCR and western blotting, respectively. Representative images of western blotting (**b**, left). **c**, Total m^{6}A levels in HaCaT and HaCaT-T cells with introduction of siMETTL3 and siControl were determined by EpiQuik m^{6}A RNA Methylation Quantification Kit. **d**, Cell viability of HaCaT and HaCaT-T cells with different treatments was tested by MTT assay. **e**, Representative images of apoptosis tested by flow cytometry (up) and quantification of cell apoptosis in HaCaT cells and HaCaT-T cells with induction of two siMETTL3 (siMETTL3–1 and siMETTL3–2) and siControl (down). **f**, Representative images of cell migration examined by wound healing assay with a microscope at 400× magnification (up) and quantification of migration in HaCaT cells and HaCaT-T cells with induction of two siMETTL3 (siMETTL3–1 and siMETTL3–2) and siControl (down). For **a**-**f**, n = 3 biological replicates, error bars indicate mean ± SEM. The *P*-values were determined by two-tailed t-test. "*" indicates a significant difference compared to control group ($P < 0.05$).

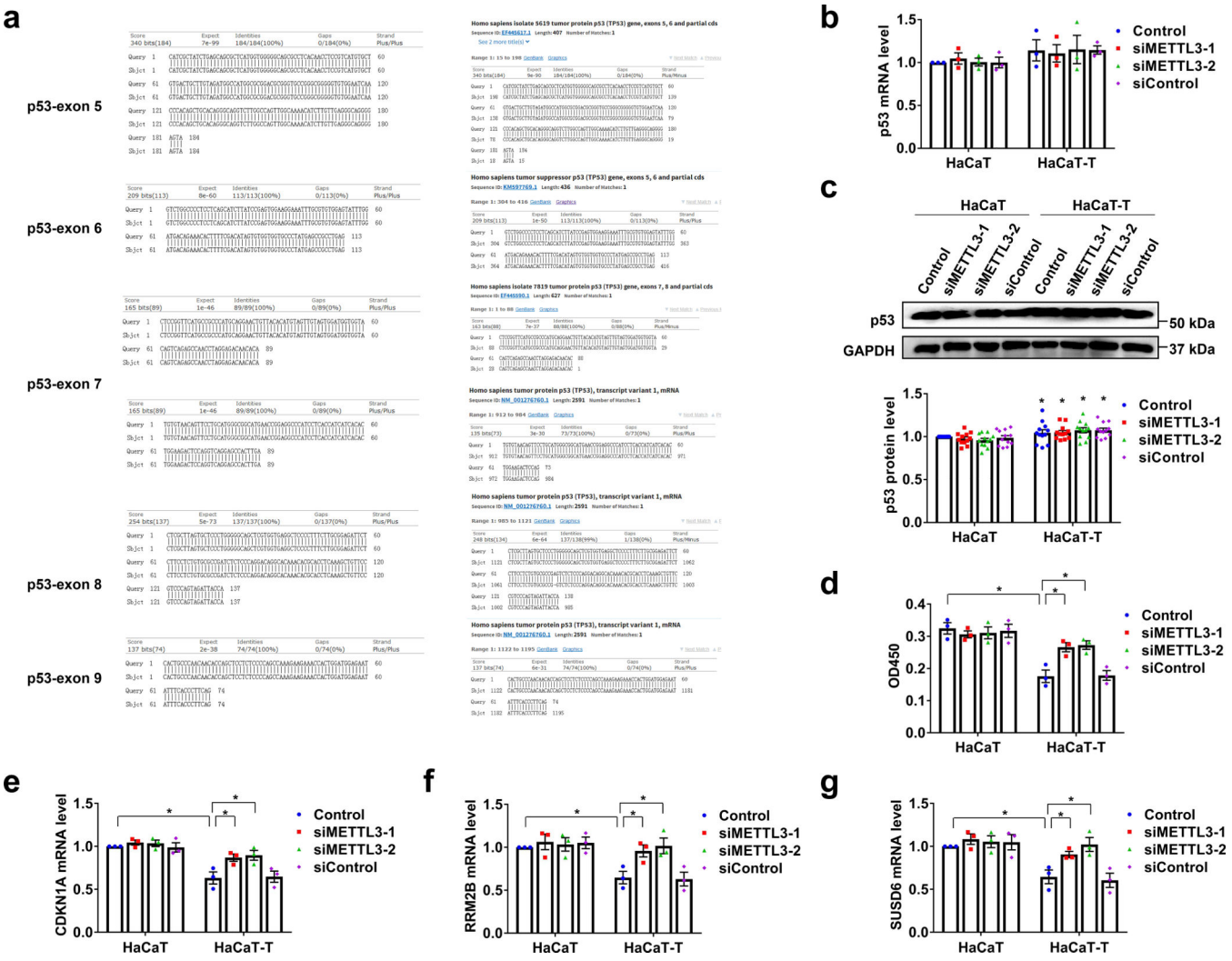

Fig. 3. p53 mutation, expression, activity, and target genes level in arsenite-transformed keratinocytes.

a, The sequence of p53 gene (exons 5–9) in HaCaT and HaCaT-T cells was detected by sequencing. **b-d**, The mRNA (**b**) and protein (**c**) levels and activity (**d**) of p53 in HaCaT and HaCaT-T cells after the indicated treatments. Representative images of western blotting (**c**, up). **e-g**, The mRNA levels of three p53 specific target genes including *CDKNA1* (**e**), *RRM2B* (**f**), and *SUSD6* (g) were examined by RT-qPCR. For **b-g**, At least 3 biological replicates, error bars indicate mean ± SEM. The *P*-values were determined by two-tailed t-test. "*" indicates a significant difference compared to control group ($P < 0.05$).

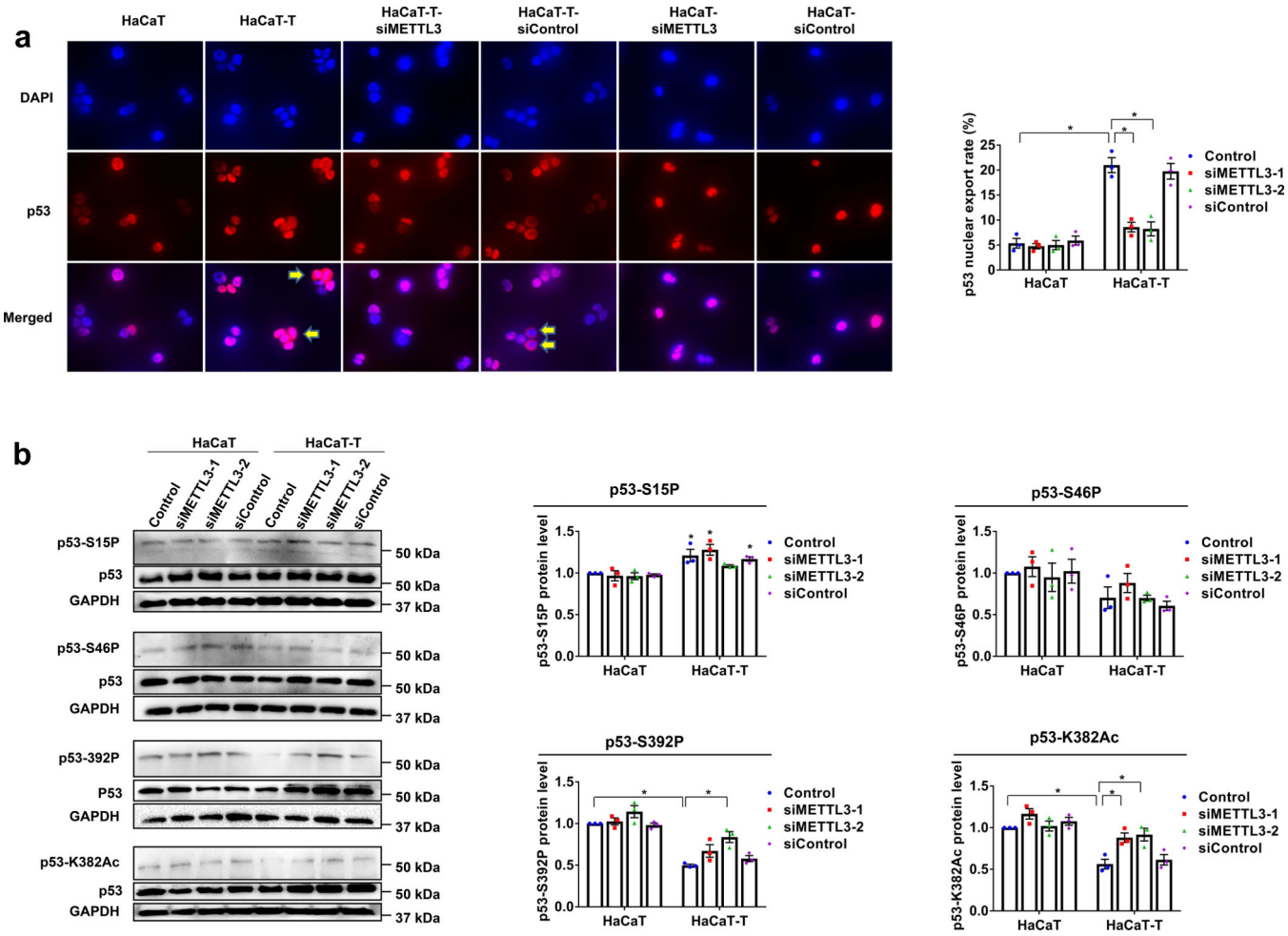

Fig. 4. m^{6}A methylation reduces p53 activation in HaCaT-T cells

a, The localization of p53 protein (red) and nucleus (blue) detected by immunofluorescence was observed with a fluorescent microscope at 400× magnification and merged by Adobe Photoshop. Cytoplasmic p53 staining is depicted by the yellow arrows (left). Quantification of p53 nuclear export rates (right). **b**, Phosphorylation levels of p53 at Ser15 site, Ser46 site, Ser392 site and p53 acetylation at Lys382 were determined by western blotting in HaCaT and HaCaT-T cells after the indicated treatments. The representative images of protein levels in p53-S15P, p53-S46P, p53-S392P, p53-K382Ac, p53 and GAPDH (left). For **a**, **b**, n = 3 biological replicates, error bars indicate mean ± SEM. The *P*-values were determined by two-tailed t-test. "*" indicates a significant difference compared to control group ($P < 0.05$).

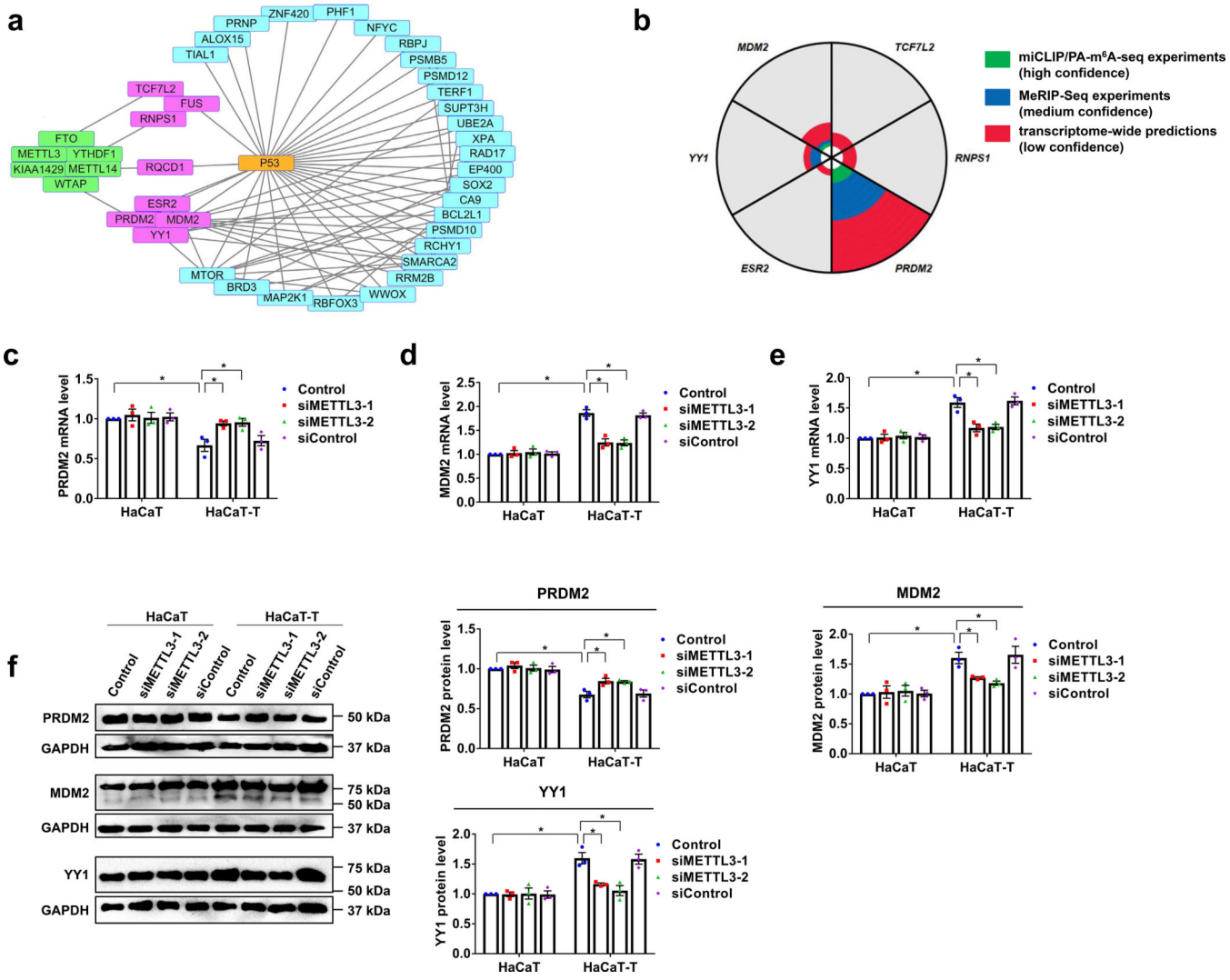

Fig. 5. Three p53 regulators are affected by m^{6}A methylation in HaCaT-T cells

a, Protein relation analysis on m^{6}A regulating proteins, p53, and genes with altered expressions in HaCaT cells after chronically exposed to low dose of $NaAsO_2$ (GSE97303) was performed by String. The genes in pink and blue rectangles differentially express in HaCaT cells chronically exposed to $NaAsO_2$ compared to HaCaT cells. The proteins in green rectangles are m^{6}A regulating proteins. The genes in pink rectangles are involved in $NaAsO_2$-induced malignant transformation and associated with m^{6}A methylation and p53. Straight lines represent two molecules are close related. **b**, The analysis of m^{6}A sites in genes which are involved in $NaAsO_2$-induced malignant transformation and associated with m^{6}A and p53 was performed in m^{6}AVAR. The “green” means there are m^{6}A sites in this gene from miCLIP/PA-m^{6}A-seq experiments with high confidence. The “blue” indicates there are m^{6}A sites in this gene from MeRIP-Seq experiments which is medium confidence. The “red” suggests there are m^{6}A sites in this gene from transcriptome-wide predictions with low confidence. The area of “green”, “blue”, or “red” represents the relative counts of m^{6}A sites in this gene. **c-e**, The mRNA levels of three genes including *PRDM2* (**c**), *MDM2* (**d**), and *YY1* (**e**) were tested by RT-qPCR in HaCaT and HaCaT-T cells with introduction of

two siMETTL3 (siMETTL3–1 and siMETTL3–2) and siControl. **f**, The representative images of PRDM2, MDM2, YY1, and GAPDH protein (left). Quantitative protein levels of PRDM2, MDM2, and YY1 protein in HaCaT and HaCaT-T cells with introduction of METTL3 siRNA were detected by western blotting (right). For **c-f**, n = 3 biological replicates, error bars indicate mean ± SEM. The *P*-values were determined by two-tailed t-test. "*" indicates a significant difference compared to control group ($P < 0.05$).

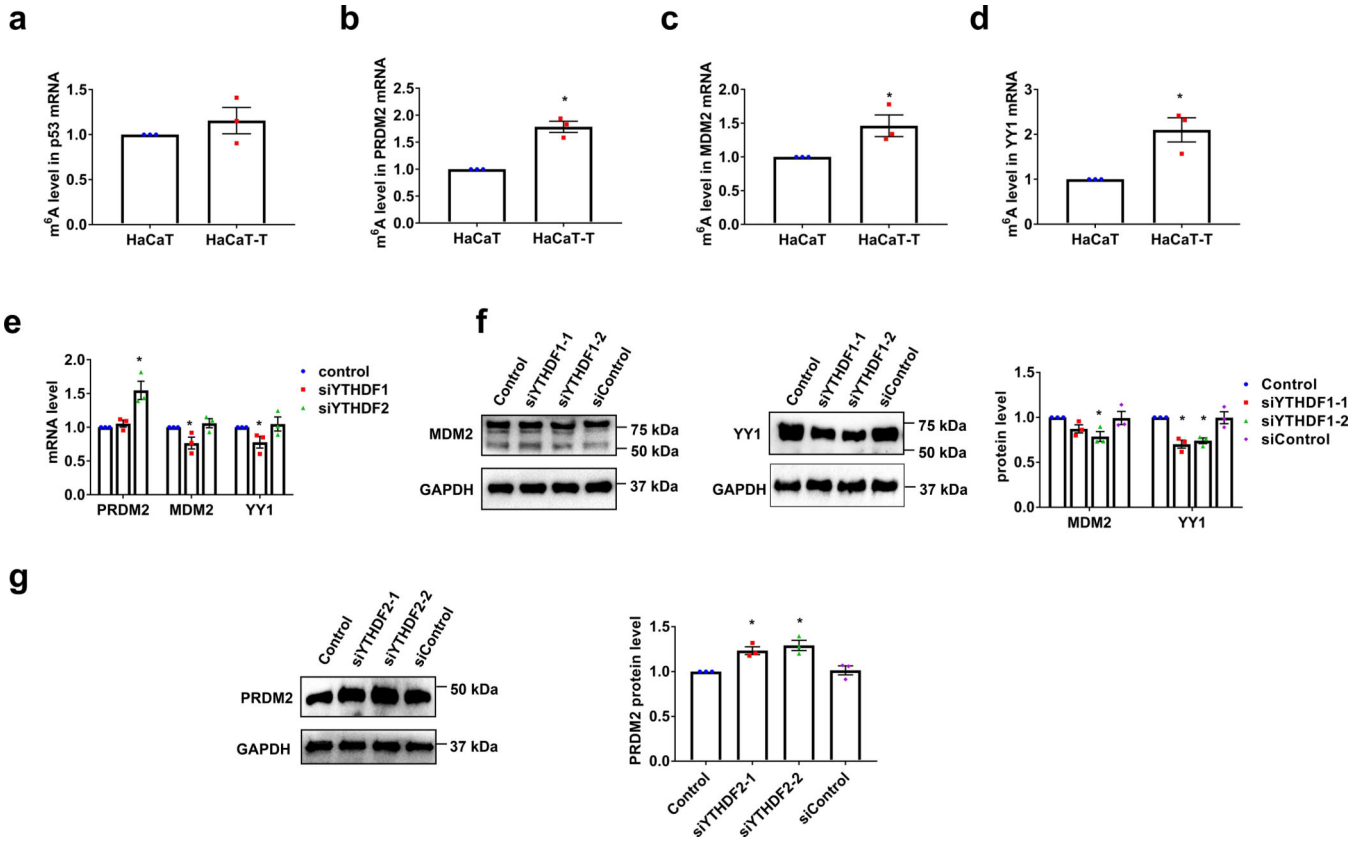

Fig. 6. m^{6}A methylation inhibits PRDM2 expression and increases MDM2 and YY1 levels in HaCaT-T cells

a-d, m^{6}A levels in *p53* (**a**), *PRDM2* (**b**), *MDM2* (**c**), and *YY1* (**d**) mRNA of HaCaT and HaCaT-T cells were determined by MeRIP. **e**, The mRNA levels of *PRDM2, MDM2,* and *YY1* in HaCaT-T cells with introduction of YTHDF1 siRNA (siYTHDF1) or YTHDF2 siRNA (siYTHDF2) were tested by RT-qPCR. **f**, The representative images of MDM2 (left) and YY1 (middle) in HaCaT-T cells with introduction of two YTHDF1 siRNA (siYTHDF1–1 and siYTHDF1–2). Quantitative protein levels of MDM2 and YY1 in HaCaT-T cells with introduction of two YTHDF1 siRNA were detected by western blotting (right). **g**, The representative images (left) of PRDM2 in HaCaT-T cells with introduction of two YTHDF2 siRNA (siYTHDF2–1 and siYTHDF2–2). Quantitative protein levels of PRDM2 in HaCaT-T cells with introduction of two YTHDF2 siRNA were detected by western blotting (right). For **a-g**, n = 3 biological replicates, error bars indicate mean ± SEM. The *P*-values were determined by two-tailed t-test. "*" indicates a significant difference compared to control group ($P < 0.05$).

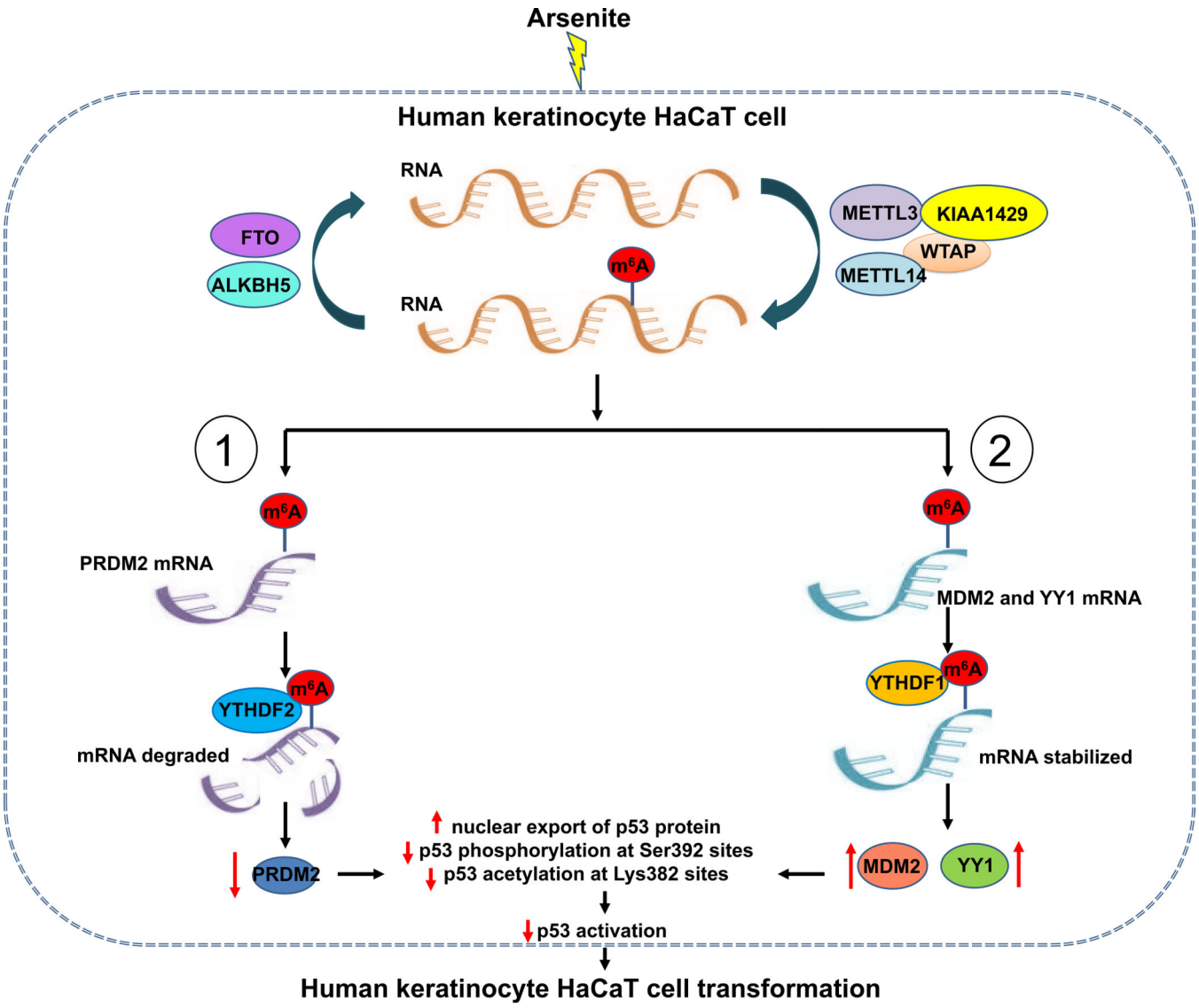

Fig. 7. Model that elevated m^{6}A methylation inhibits p53 activation to mediate arsenite-induced human keratinocytes transformation

Chronical exposure of arsenite induces the overexpression of m^{6}A methyltransferases (METTL3, METTL14, WTAP, and KIAA1429) and the attenuation of m^{6}A demethylases (FTO), leading to elevated m^{6}A methylation level in transformation of human keratinocytes. Upregulated m^{6}A methylation in p53 positive regulator *PRDM2* mRNA binds with m^{6}A reader YTHDF2, inducing the degradation of *PRDM2* mRNA and inhibition of PRDM2 expression. Whereas high levels of m^{6}A methylation in p53 negative regulator *MDM2* and *YY1* mRNA combines with m^{6}A reader YTHDF1, promoting the stabilization and translation of *MDM2* and *YY1* mRNA. The suppression of p53 positive regulator and the increase of p53 negative regulators induced by m^{6}A methylation contribute to p53 inactivation involved in arsenite-caused transformation.